Available online at www.sciencedirect.com
ScienceDirect
Polymer 48 (2007) 6691–6706
polymer
www.elsevier.com/locate/polymer

Overload effect on the fatigue crack propagation of PC/ABS alloy

Qin-Zhi Fang, T.J. Wang*, H.M. Li

MOE Key Laboratory for Strength and Vibration, Department of Engineering Mechanics, Xi'an Jiaotong University, Xi'an 710049, China

Received 1 April 2007; received in revised form 28 July 2007; accepted 15 August 2007
Available online 23 August 2007

Abstract

The effect of single overload within an otherwise constant amplitude loading sequence on the fatigue crack propagation (FCP) behavior of the alloy of polycarbonate and acrylonitrile–butadiene–styrene (PC/ABS) is experimentally investigated in this paper. An improved compliance method is employed to measure the fatigue crack length of the specimen. Optical and scanning electron microscopes are used to observe the features of crack surface and the process of crack tip deformation. The overload waveform has slight effect, while the overload ratio has great effect on the crack growth retardation. A small crack increment is produced during overloading. The crack growth rate reduces quickly, and then increases gradually until it reaches the steady crack growth rate level when the loading recovers to normal constant amplitude fatigue loads. Porous or dimple features govern the fatigue crack surfaces.

Keywords: Fatigue crack propagation; Overload effect; PC/ABS alloy

1. Introduction

Fatigue failure is one of the main failure modes in engineering structures. Polymers are being widely used in some important engineering structures, such as the structures in aerospace, automobile, pressure vessels and pipes, etc. Therefore, investigation of the fatigue and fracture of polymers will be important and extensive researches have been devoted to this field. Several researches studied the effects of loading parameters and microstructures on the fatigue crack growth behaviors of polymers [1–12]. Bretz et al. [1] proposed a cyclic damage mechanism to explain the crack tip deformation patterns. A simple viscoelastic model was presented to explain the strong influence of molecular weight on fatigue crack propagation rates [2]. Furmanski and Pruitt [10] used the maximum stress intensity factor rather than the stress intensity range to describe the fatigue crack propagation behavior of ultra-high molecular weight polyethylene (UHMWPE). Pruitt and Bailey [11] and Baker et al. [12] studied the effects of polymer processing procedures. The effects of manufacturing process (compress molding or ram extrusion), sterilization, aging environment and notch orientation relative to the extrusion direction on the fatigue crack propagation of polymers were studied. The effect of specimen shape and dimension was also investigated [13,14]. Shah et al. [13] studied the correlation of the fatigue crack propagation in polyethylene (PE) pipe with different specimen geometries. Also, the slow crack propagation in a real PE pipe was experimentally studied through fatigue test with compact tension (CT) specimens [14]. Parsons et al. [15] experimentally studied the damaged zone ahead of the arrested crack in high and medium density polyethylene (HDPE and MDPE). It was shown that the shape of the damaged zone had great influence on the crack growth properties of these materials. The features of the fatigue crack surfaces were different with different crack growth rates. Discontinuous crack growth bands (DGBs) appeared on the crack surface at low fatigue crack growth rates which associated with crazed material in the plastic zone, dimple structures appeared on the fracture surfaces at moderate fatigue crack growth rates, and striation structures were found on the fracture surfaces at high fatigue crack growth rates [15–20].

* Corresponding author. Tel./fax: +86 29 8266 5168.
E-mail addresses: fangqz@mail.xjtu.edu.cn (Q.-Z. Fang), wangtj@mail.xjtu.edu.cn (T.J. Wang).

0032-3861/$ - see front matter © 2007 Elsevier Ltd. All rights reserved.
doi:10.1016/j.polymer.2007.08.048

The retardation of fatigue crack growth induced by an overload has been studied for metals and composite materials [21–24]. The damage accumulation mechanism is different in composites and metals. There is no retardation effect after tensile overload in composites; however, there is obvious retardation effect on crack propagation in metals. For metals this phenomenon is caused by the formation of relatively large zone of residual compressive stress in front of a crack tip after the application of overloading. There are a few researches on the overload effect on crack propagation of polymers [25–28]. Mai [25] suggested that the crack retardation was due primarily to the formation of crazes thus blunting the crack tip after the overload. Imai et al. [27] experimentally studied the retardation of fatigue crack growth due to overload in polymethylmethacrylate (PMMA) by measuring the optical interference fringes from the crack and craze during the fatigue loading with a very low cyclic fatigue frequency, and concluded that the reduction of the stress at the crack tip after removing the overload was one of the main reasons that caused the retardation of crack growth. Yuen et al. [28] studied the effects of loading frequency, tensile overload and compressive underload on the fatigue crack propagation of PMMA. It was shown that the crack propagation accelerated when the overload was applied, and retardation occurred when the overload was removed. Here it should be noted, unlike metals, crack closure is not the only reason for the retardation of crack growth in polymers. It is still an open problem to study the effect of overload on the retardation of polymer fatigue crack propagation.

The objective of the current work is to experimentally investigate the overload effect on the FCP behavior of PC/ABS alloy. To this end, an improved compliance method [29] is employed to measure fatigue crack propagation. Effects of the overload ratio (P_{peak}/P_{max}) and overload waveform on the FCP behavior of PC/ABS alloy are discussed in detail. In situ observations of the overload effect on the FCP behavior of these materials are also presented. Fatigue crack tip deformation and the fatigue crack surfaces are observed by using optical and scanning electron microscopes, and some interesting features are obtained.

2. Experimental

2.1. Materials and specimens

The material considered here is PC/ABS alloy. The average molecular weight of PC is 26,000 g/mol. SWA compatibilizer is added to the blend of PC and ABS before injection. The composition of the PC/ABS alloy is 66/30/4 PC/ABS/SWA. The pellet sizes are mainly consists of 0.2–0.5 μm in diameter. The injection temperature of the PC/ABS plate is 240–250 °C. The holding pressure is 60–80 MPa.

According to the standard ASTM E-647, compact tension (CT) specimens with thickness B of 2.8 mm, width W of 50 mm, notch depth of 15 mm and notch opening width of 2 mm, as shown in Fig. 1(a), are designed. The specimens are carefully manufactured from PC/ABS plates with dimensions of 167 mm × 102 mm × 3 mm. Before fatigue testing, a small pre-crack of 1.5–2 mm at the notch tip for each specimen is manually introduced by slowly pushing a fresh razor blade into the specimen along the notch direction. The initial crack length a_0 is about 17 mm. To have a closer observation of the micro-mechanisms of fatigue fracture in polymers, single edge cracked eccentric tension specimens as depicted in Fig. 1(b) are cut from the fatigue cracked CT specimens. Then, the single edge cracked specimens with an initial fatigue crack of about 4 mm in length are used for in situ scanning electronic microscope (SEM) observation of FCP mechanism during and after an overload application.

2.2. Experimental procedures

A computer-controlled INSTRON-5848 machine is used for fatigue crack propagation (FCP) tests at room temperature (about 24 °C) in air.

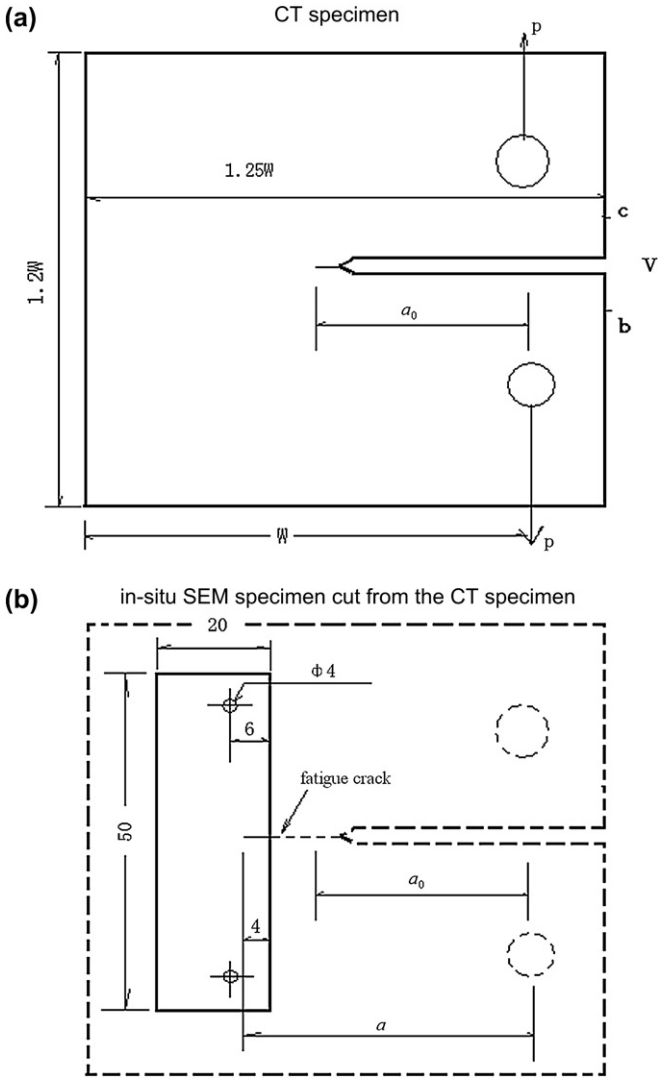

Fig. 1. Geometry and dimensions of the specimens with w being the width of specimen, V the displacement measured by the displacement gage mounted on the specimen between b and c, P is the fatigue load.

To investigate the effect of overload ratios on the FCP rate of the polymers, single overload within an otherwise constant amplitude loading sequence is applied to specimens during fatigue crack growth tests. It is shown in previous tests that the manual interruption of fatigue test would have some effects on the fatigue crack growth test results for some polymer materials. Because the fatigue loads are generally small in these kinds of test for polymers, unexpected overloadings are often introduced if the fatigue test is manually interrupted. Therefore, to avoid the influence of these loading operations, the fatigue loading process is previously programmed for the overload fatigue test. Two different overload waveforms are used in the present test. Fig. 2(a) and (b) gives a depiction of the fatigue blocks as well as the overload waveforms. As shown in Fig. 2, for the overload cycle, the maximum load is P_{peak} and the frequency is 0.005 Hz for sinusoidal waveform, the holding time $t_h = 60$ s and loading and unloading time $t_r = 5$ s for trapezoidal waveform. Blocks 1 and 2 are constant fatigue load blocks with a constant amplitude sinusoidal waveform fatigue loading ($P_{max} - P_{min}$) at a frequency and load ratio R ($=P_{min}/P_{max}$) of 3 Hz and 0.1, respectively. The maximum load P_{max} and the minimum load P_{min} in the base fatigue blocks 1 and 2 are chosen so that the fatigue crack growth rates are in a reasonable range ($3-8\times10^{-5}$ mm/cycle). These are within the range of FCP rates that are frequently used in literature [11–20,25–28]. The loading cycles in block 1 are chosen so that a fatigue crack length increment of about 2 mm can be reached in the fatigue loading block, and the FCP process can get out of its initiation stage, and arrive to a normal FCP level. It is intended to choose such a long loading cycles in block 2 that the fatigue crack can be ensured to propagate out of the overload-affected zone in the block.

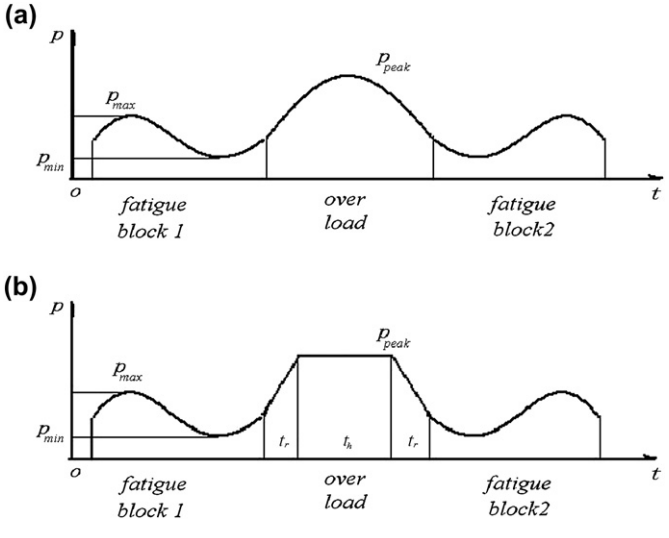

Fig. 2. Fatigue-overload patterns. Overload cycle with (a) sinusoidal waveform and (b) trapezoid waveform. The blocks 1 and 2 are constant amplitude fatigues with different cycles. The maximum and the minimum loads for the fatigue blocks are P_{max} and P_{min}, respectively. The maximum load for overload cycle is P_{peak} with frequency of 0.005 Hz for the sinusoidal waveform, and holding time $t_h = 60$ s and the loading and unloading time $t_r = 5$ s for trapezoid waveform, respectively.

However, because the effect of overload on the FCP is not clear, it is not easy to choose proper loading cycles for block 2 before testing. Generally, trial and error are needed to give proper loading cycles for fatigue blocks 1 and 2. They are generally more than 50,000 depending on the value of overload ratio P_{peak}/P_{max} for PC/ABS alloy. Reference to literature [27,28]: P_{peak}/P_{max} value of 1.18 is used in the experiment given in Ref. [27], which gives a retardation of about 60 cycles. P_{peak}/P_{max} values of 1.7 and 1.95 are used in the experiment in Ref. [28], which gives overload retardation cycles of about 1000 cycles. To obtain an obvious effect of overload ratio on FCP retardation, two overload ratios of 2.5 and 3 are used in the investigation. With these considerations, the amplitudes of base fatigue loads P_{min} and P_{max} are chosen as 6 N and 60 N, respectively, which correspond to a FCP rate range of $3-8\times10^{-5}$ mm/cycle. The peak values of overload are 150 N and 180 N, which correspond to the overload ratio $P_{peak}/P_{max} = 2.5$ and 3, respectively.

The variation of on-line crack mouth opening displacement V and load P data is collected every 300 cycles during the FCP tests, so that crack length can be obtained from compliance technique given in Ref. [29]. The crack mouth opening displacement V is measured with a clip gage mounted on the CT specimen with a gage length of 10 mm, at points b and c as shown in Fig. 1. Besides, a traveling visual microscope is also used to follow the crack propagation, which can provide a calibration for the crack length obtained from compliance technique. The crack tip deformation can be observed too with the traveling visual microscope.

JSM-35C SEM equipped with fatigue loading device is used for the observation of the crack tip deformation during fatigue loading with the small specimens as shown in Fig. 1(b). The loading frequency and stress ratio are 0.08 Hz and $R = 0.1$, respectively for the in situ small specimens. On the other hand, the overload effects on the fracture surfaces of fatigue specimens are observed in JSM-35C SEM and Quanta 400 environmental SEM.

2.3. Calculation of FCP rate

The crack length during fatigue test is measured by using an improved compliance method. The curves of load P vs displacement V are recorded from the INSTRON-5848 machine. ASTM E-399 standard allows one to use the following formula to calculate the dimensionless compliance $BE'\Delta V/\Delta P$ for CT specimen,

$$\frac{BE'\Delta V}{\Delta P} = \frac{19.75}{(1-a/W)^2}\left[0.5 + 0.129\left(\frac{a}{W}\right) + 1.385\left(\frac{a}{W}\right)^2 - 2.919\left(\frac{a}{W}\right)^3 + 1.842\left(\frac{a}{W}\right)^4\right] \quad (1)$$

where B is the thickness of specimen, E' – elastic modulus of material and $E' = E$ for plane stress and $E' = E/(1-\nu^2)$ for plane strain with ν – Poisson's ratio and E – Young's modulus of material, a – length of crack, W – the width of specimen,

ΔV and ΔP are the increment of the crack opening displacement and load, respectively, obtained from the cyclic load displacement curve. Generally, E' should be determined according to the crack length calibration. With this technique, one can obtain the (a, N) data from compliance technique given in Ref. [29].

According to the standard ASTM E-647, one can calculate the amplitude of stress intensity factor (SIF) ΔK and FCP rate by using the measured data of a and N,

$$\Delta K = \frac{\Delta P}{B\sqrt{W}} \frac{2 + a/W}{(1 - a/W)^{3/2}} \left[0.866 + 4.64\left(\frac{a}{W}\right) - 13.32\left(\frac{a}{W}\right)^2 + 14.72\left(\frac{a}{W}\right)^3 - 5.6\left(\frac{a}{W}\right)^4 \right] \quad (2)$$

and then the well-known Paris law

$$\frac{da}{dN} = C(\Delta K)^m \quad (3)$$

can be employed to quantitatively describe the FCP rate, in which C and m are material constants.

Using the (a, N) data pairs, fatigue loading data and seven-point formula deductive technique, a computer program is written to obtain the FCP rate of PC/ABS alloy. By inputting the values of E', the initial crack length a_0, the dimensions of specimen, the fatigue load, crack opening displacement, the number of fatigue cycles, one can obtain the data (a, N) and $(da/dN, \Delta K)$, simultaneously. Also, the curves of $a-N$ and $da/dN-\Delta K$ can be obtained.

3. Results and discussions

3.1. Fatigue crack propagation process

To verify the suitability of the crack growth measurement, comparison of the crack length measured from the improved compliance method and visual microscope method is made for some specimens. Fig. 3 shows an example of the comparison of the $a-N$ curves for a specimen fatigue cracked with constant sinusoidal waveform fatigue loading, where P_{min} and P_{max} are 6 N and 60 N, respectively, and the frequency is 3 Hz. Fig. 4(a) and Fig. 6(a) show the comparison of $a-N$ curves for specimens, which are tested with an overload applied within an otherwise constant fatigue loading. It is shown that excellent agreement can be seen both for FCP test with and without overload in constant fatigue loading. It is clear that the improved compliance method has enough accuracy to measure the fatigue crack length, which can greatly reduce testing time and experimental errors.

In what follows, the improved compliance method is employed to measure the $a-N$ curves of PC/ABS alloy under various fatigue loadings. Using the $a-N$ data, Eq. (2) and the software mentioned above, we can easily obtain the curve of $da/dN-\Delta K$ for PC/ABS alloy.

Fig. 4(a) shows the $a-N$ curve of specimen PC/ABS1-24 of fatigue cracked with a sinusoidal waveform overload applied within an otherwise constant fatigue loading. The normal fatigue loads P_{min} and P_{max} are 6 N and 60 N, respectively. The maximum of the sinusoidal waveform overload is 150 N, which corresponds to an overload ratio of 2.5. Correspondingly, the photos in Fig. 4(b)–(g) show the in situ optical observation of the fatigue crack tip deformation process of the specimen before and after overloading with an overload of 150 N. It should be noted that the clip-like feature shown in the photos is only part of the plastic zone for each overload. It is only a reflection picture of the plastic zone due to the different reflection features on specimen surface. The real shape of plastic zone is a shallow oval ahead of the crack tip, which is a little larger than the brighter oval zone ahead the crack tip. Fig. 4(b) shows the crack tip deformation when the fatigue cycle approaches 150,000, just before the overload being applied. The crack tip has a normal small plastic zone, and the FCP rate is about 8×10^{-5} mm/cycle. The plastic deformation near the fatigue crack surfaces is slim and steady. Fig. 4(c) shows the crack tip deformation with large plastic zone during the overload application. After that, the fatigue load is recovered to the normal constant load, where the maximum and minimum loads are 60 N and 6 N, respectively. After another 216 cycles, the crack tip plastic zone is a little bit larger than before, and a small crack extension is observed. Fig. 4(d) shows the crack tip plastic zone at 150,216 cycles. That means the plastic zone has extended during the fatigue loading just after the overload. This is due to the time dependent plastic deformation properties of polymer. Then, the crack does not grow until the fatigue cycles approach 167,128. A slight crack extension is observed and the crack path has changed due to the effect of overload, as shown in Fig. 4(e). Gradually, the FCP rate increases slowly with the increasing of fatigue cycle, and the crack extends obviously, as shown in Fig. 4(f) and (g). Fig. 5 shows a close observation of the crack propagation in the overload-affected plastic zone. It is readily seen that the crack propagation wakes look thinner in the overload plastic zone than that in the normal crack growth region, which means

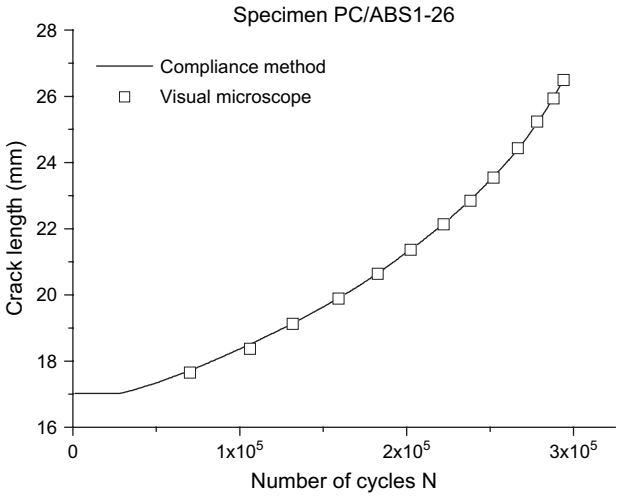

Fig. 3. Comparison of the measured $a-N$ curves for a specimen with constant sinusoidal wave fatigue load cycles, where P_{min} and P_{max} are 6 N and 60 N, respectively, and the frequency is 3 Hz.

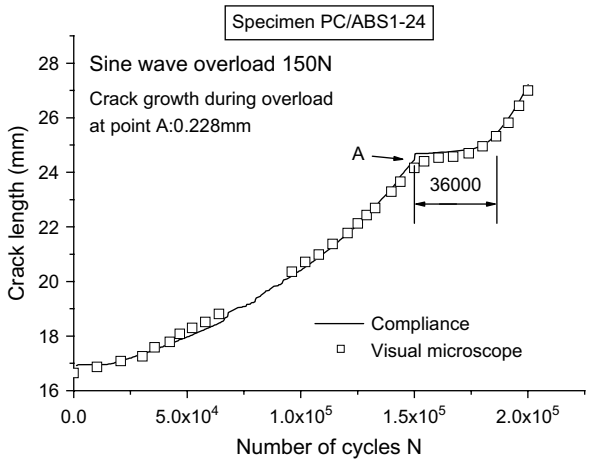

(a) On the *a*~*N* curve

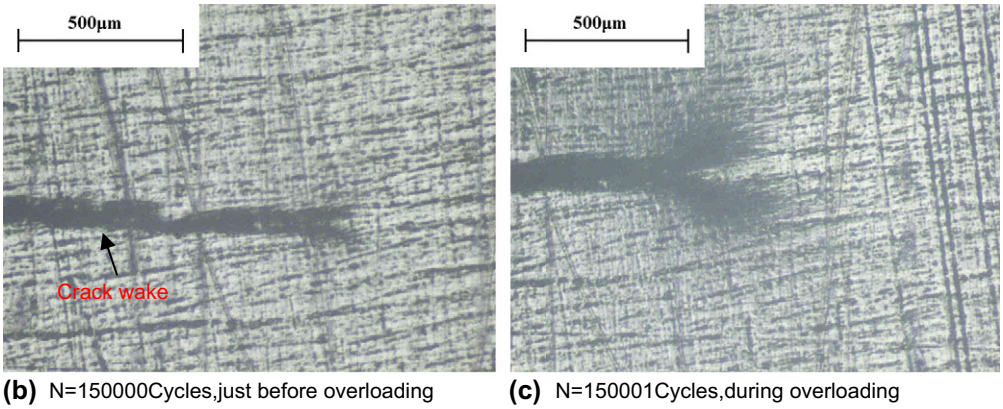

(b) N=150000Cycles,just before overloading

(c) N=150001Cycles,during overloading

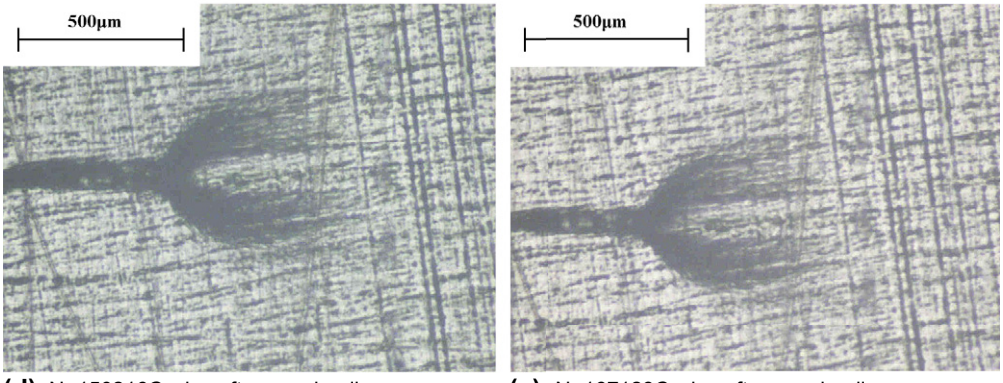

(d) N=150216Cycles,after over loading

(e) N=167128Cycles,after over loading

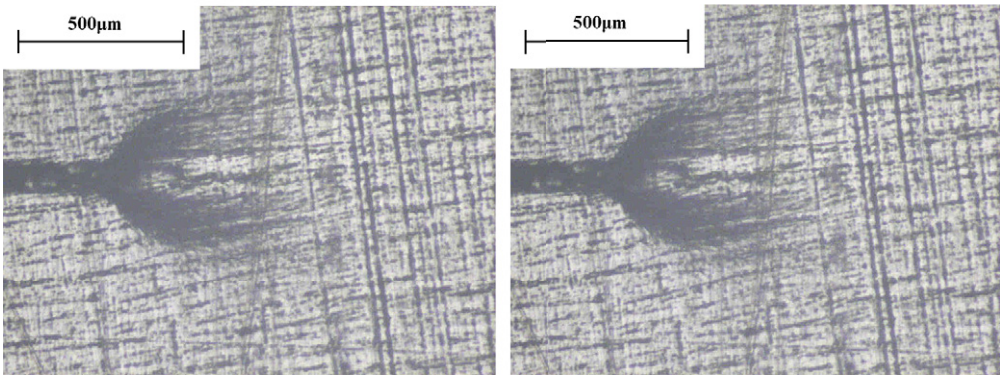

(f) N=174001Cycles,crack appears

(g) N=178023Cycles,crack propagates

Fig. 4. Effect of sinusoidal wave overload ($P_{peak}/P_{max} = 2.5$) on the crack growth retardation of PC/ABS alloy. (a) On the a–N curve; (b) $N = 150{,}000$ cycles, just before overloading; (c) $N = 150{,}001$ cycles, during overloading; (d) $N = 150{,}216$ cycles, after overloading; (e) $N = 167{,}128$ cycles, after overloading; (f) $N = 174{,}001$ cycles, crack appears; and (g) $N = 178{,}023$ cycles, crack propagates.

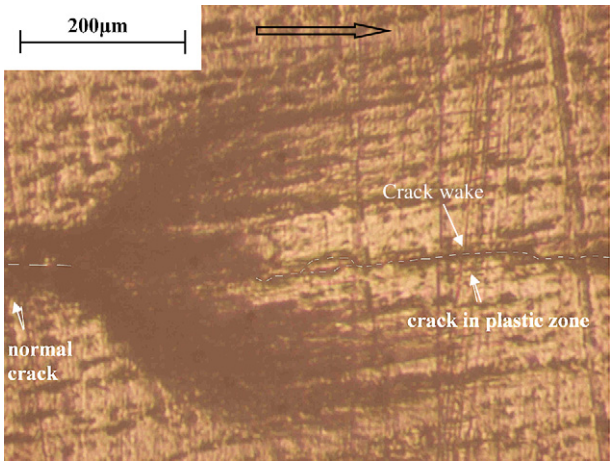

Fig. 5. Crack propagation in the overload plastic zone.

that the crack growth rate is lower and the effective fatigue load range is smaller than that in the normal constant amplitude loading.

Fig. 6(a) shows the $a-N$ curve of specimen PC/ABS1-23 of fatigue cracked with a trapezoid waveform overload applied within an otherwise constant fatigue loading. The normal fatigue loads P_{min} and P_{max} are also 6 N and 60 N, respectively. The maximum of the trapezoid waveform overload is 150 N. Correspondingly, the photos in Fig. 6 show the in situ optical observation of the fatigue crack tip deformation process of the specimen before and after the overloading. Similar crack tip deformation and fatigue crack propagation processes are observed in these photos, except that the increasing of the crack tip plastic deformation is recorded in Fig. 6(c) and (d). The normal steady plastic wakes can be observed in Fig. 6(b)–(d). The crack tip plastic zone extends with the increasing load, as shown in Fig. 6(c) and (d). The crack tip plastic zone reaches its maximum at the end of the high level load holding time with the load of 150 N (Fig. 6(d)). After that, the normal sinusoidal waveform fatigue load of 6 N–60 N is applied to the specimen again, and the plastic zone looks a little smaller (Fig. 6(e)). Then, the crack does not propagate after another 40,000 fatigue cycles (Fig. 6(f)). Gradually, the FCP rate increases with increasing fatigue cycle, and the crack propagates obviously, as shown in Fig. 6(g) and (h). It can also be seen that the crack propagation wake is thinner in the overload plastic zone than that in the normal crack growth region (Fig. 6(h)).

Fig. 7(a) shows the $a-N$ curve of specimen PC/ABS1-25 of fatigue cracked with three-time sinusoidal waveform overloads (the overload ratio $P_{peak}/P_{max} = 3$) within an otherwise constant fatigue loading. Fig. 7(b) shows the corresponding crack propagation process. The crack tip plastic zones A, B and C induced by overloads (the overload ratio $P_{peak}/P_{max} = 3$) applied to the specimen correspond to the points A, B and C on the crack growth curve shown in Fig. 7(a). The first overload creates crack tip plastic zone *A*. There is no obvious crack propagation after 90,000 cycles under fatigue loading with a load range of 6 N–60 N. Then the second overload is applied, a net crack increment of 0.14 mm is induced and the crack tip plastic zone *B* is formed. No obvious crack growth is observed after another 150,000 cycles of fatigue loading. When the third overload is applied, a net crack increment of 0.18 mm is produced and the crack tip plastic zone *C* is formed. After about 200,000 fatigue cycles, the crack tip propagates beyond point D with a crack length increment of about 0.7 mm, the crack propagation rate gradually approaches the FCP rates under normal constant amplitude fatigue loading. It is shown that the fatigue crack wakes in the region beyond point D look similar to the wakes in the region D1 where the crack propagates without the influence of overloading. They are much thicker than the fatigue crack wakes in the overload-affected plastic zone, as shown between C and D.

Fig. 8(a) shows the $a-N$ curve of specimen PC/ABS1-22 of fatigue cracked with three-time trapezoid waveform overloads applied within an otherwise constant fatigue loading. Fig. 8(b) shows the corresponding crack propagation process. The crack tip plastic zones A–F induced by overload applied to the specimen correspond to point A–F on the crack growth curve shown in Fig. 8(a).

It is noted that there is a small crack increment during the application of overload, and then the retardation of crack propagation occurs after removing the overload. After the first overload of 180 N (i.e. $P_{peak}/P_{max} = 3$) being applied at point A, as shown in Fig. 8, the crack propagation is nearly stopped during the subsequent 51,000 fatigue cycles until the next overload is applied at point B, where a crack increment of 0.1 mm is produced during the overload. After that, the crack propagation is stopped again until the third overload of 180 N is applied at point C. Similar phenomena can be observed in the following overloads till point F. Also, we can see from Fig. 8 that larger net increment of crack length is measured at point D because the crack tip suffers a larger number of fatigue cycles between points C and D, which is related to a larger accumulation of fatigue damage at the crack tip. The number of fatigue cycles between points C and D is 212,516, which is larger than that between points D and E or E and F, so that the crack increment 0.25 mm at point D is larger than the crack increments 0.138 mm and 0.133 mm at points E and F, respectively. However, quantitative correlation between the crack increment and the damage state cannot be given yet. Although, the damage accumulation processes were discussed microscopically for some kinds of polymers in literature [1,15,18,27], no proper parameters were used to describe the damage accumulation state at the fatigue crack tip.

As we know, a crack would extend when the stress intensity factor K is larger than the critical stress intensity factor K_c (fracture toughness) of the material near the crack tip and stop when K is less than K_c. According to the test results for specimens PC/ABS1-22 and PC/ABS1-25, the crack stopped after a previous overloading, which means the crack intensity factor is less than K_c of the material near the crack tip at that time. Then a number of fatigue loading cycles are applied to the crack tip, and the materials around the crack tip would be damaged, and the fracture toughness K_c is reduced. The larger the fatigue loading cycles are, the lower the K_c would be. The stress intensity factor K would be larger than K_c

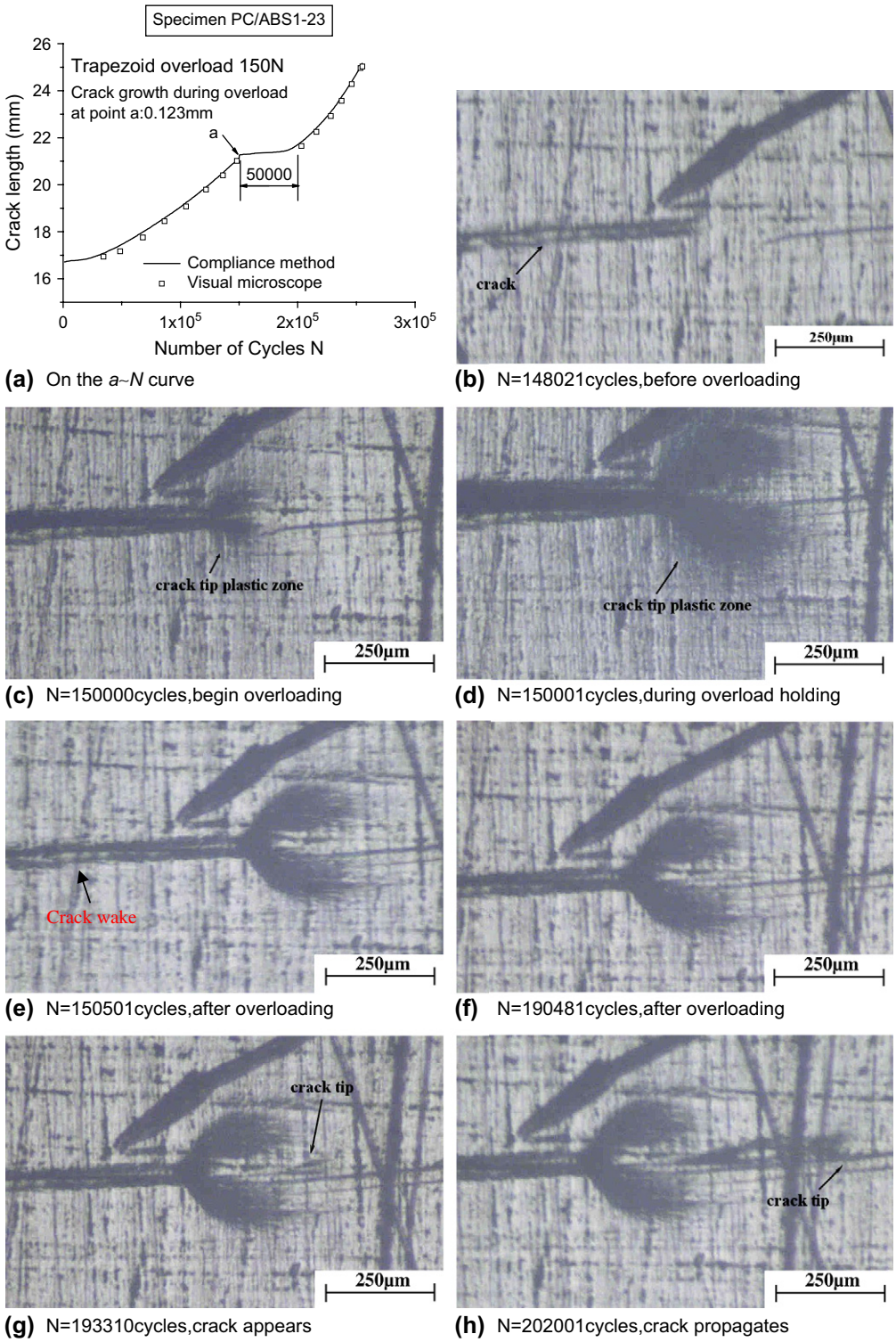

Fig. 6. Effect of trapezoid overload ($P_{peak}/P_{max} = 2.5$) on the crack growth retardation of PC/ABS alloy. (a) On the $a-N$ curve; (b) $N = 148{,}021$ cycles, before overloading; (c) $N = 150{,}000$ cycles, begin overloading; (d) $N = 150{,}001$ cycles, during overload holding; (e) $N = 150{,}501$ cycles, after overloading; (f) $N = 190{,}481$ cycles, after overloading; (g) $N = 193{,}310$ cycles, crack appears; and (h) $N = 202{,}001$ cycles, crack propagates.

when next overload is applied. Therefore, the damaged zone would fracture. The larger the damaged zone is, the lower the fracture toughness K_c of the material around the crack tip would be, and the larger the crack increment is induced by the next overload. In these experiments for specimens PC/ABS1-22 and PC/ABS1-25, because the maximum overloads are same (180 N) and the differences of the crack length during the application of overload are small (19.22–19.99 mm), the stress intensity factors during each overload could be approximately considered to be nearly same. Therefore, the length of the net crack increment can be used to reflect the damaged state at the crack tip before the application

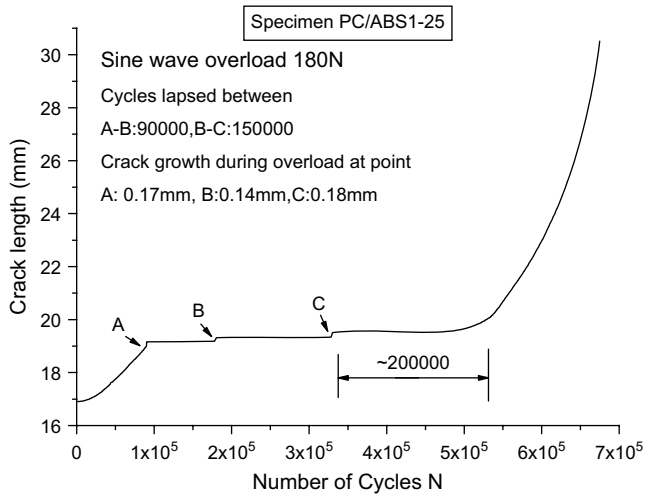

(a) Effect on the *a*~*N* curve

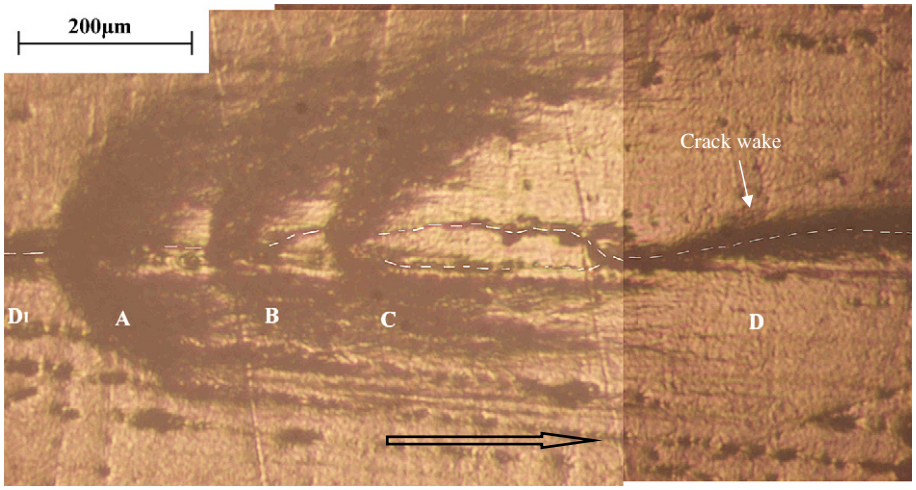

(b) Effect on the crack growth

Fig. 7. Crack tip plastic zone of the specimen under three-time overload and the effect of crack tip plastic zone on the crack propagation of PC/ABS alloy. A–C in (b) are plastic zones induced by the three-time overloads, and D the zone of crack propagation under constant amplitude fatigue load. (a) Effect on the *a*–*N* curve and (b) effect on the crack growth.

of the overload. Fig. 9 shows the net crack increment induced by the overload vs the fatigue cycles elapsed between two overloads for specimens PC/ABS1-22 and PC/ABS1-25, which correspond to trapezoidal and sinusoidal waveforms, respectively. It is shown that the net crack increments nearly increase linearly with the fatigue cycles elapsed between two overloads for each overload waveform. There is no obvious difference for these two specimens. Therefore, it can be concluded that although the crack does not propagate for certain number of fatigue cycles, the fatigue damage at the crack tip accumulates with the fatigue loading cycles. The larger the number of the fatigue loading cycles elapsed after removing the overload, the larger the damage accumulated at the crack tip is.

3.2. Fatigue crack propagation

Overload effect on the $da/dN-\Delta K$ curves of PC/ABS alloy is shown in Fig. 10 for different overload ratios P_{peak}/P_{max}.

We can learn from Fig. 10 that the larger the overload, the greater the overload effect and the lower the crack growth rate after removing the overload. It can be observed that the crack propagation rate increases during or just after the overloading cycle. According to the *a*–*N* curves, the higher values of FCP rate are mainly due to the net increment of crack length induced by the overload. After removing the overload, the crack growth rate quickly reduces to a low level and then increases gradually with fatigue cycles, and finally approaches a normal FCP rate level of constant amplitude fatigue.

We can learn from Figs. 7 and 8 that the crack propagates only a very small value before the next overload cycle is applied. This is because the interval between each two three-time overloads is not large enough. The crack growth rate stays at very low levels until the crack propagates out of the overload-affected zone.

It is reasonable to describe the overload effect with an overload retardation ratio N_r/N_n. Here N_r is the fatigue loading cycle needed to cover an overload-affected crack increment, and

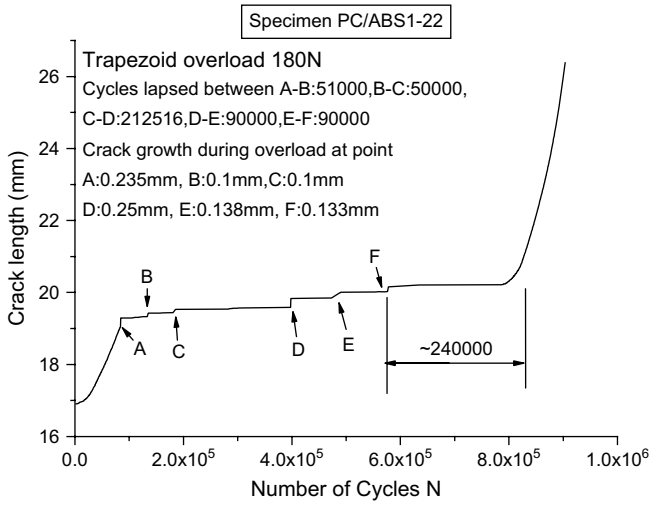

(a) Effect on the *a*~*N* curve

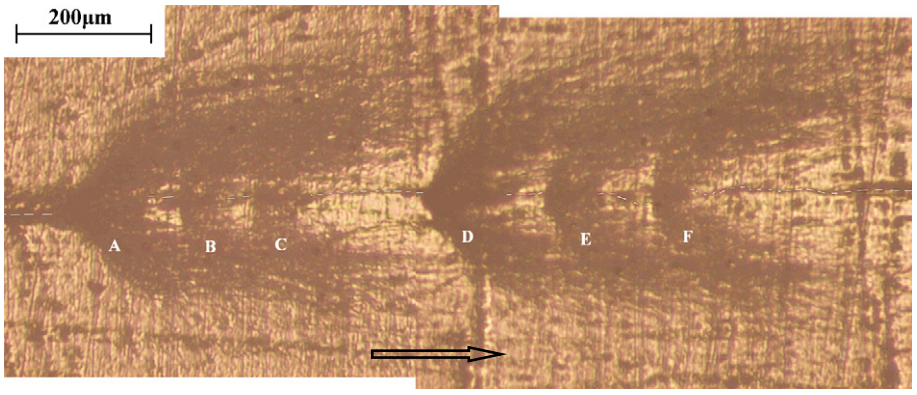

(b) Effect on the crack growth

Fig. 8. Effect of trapezoid overload ($P_{peak}/P_{max} = 3$) on the crack growth retardation of PC/ABS alloy. (a) Effect on the a–N curve and (b) effect on the crack growth.

N_n is the fatigue loading cycle needed to cover the corresponding overload-affected crack increment under normal fatigue loading condition. According to Fig. 10(a), the normal crack growth rates da/dN near the points where overloads are applied are 4.85×10^{-5} and 1.07×10^{-4} mm/cycle for specimens PC/ABS1-23 and PC/ABS1-24, respectively. With a–N data obtained in the tests, the crack increments needed for the crack growth rate to recover the normal crack growth rates after the overload retardation are 0.58 mm and 0.96 mm for specimens PC/ABS1-23 and PC/ABS1-24, respectively. Therefore, the fatigue cycles N_n needed to cover the crack increments can be calculated to be 1.19×10^4 and 8.972×10^3 cycles for specimens PC/ABS1-23 and PC/ABS1-24, respectively. As shown in Figs. 4 and 6, the cycles N_r needed to cover the corresponding crack increments 0.58 mm and 0.96 mm (the overload-affected crack increment) in the tests are 50,000 and 36,000 cycles, therefore the overload retardation ratios N_r / N_n can be obtained to be 4.202 and 4.012 for specimen PC/ABS1-23 and specimen PC/ABS1-24 which correspond to the overload waveform of trapezoid and sinusoid, respectively. As shown in Figs. 7 and 8, for the specimens PC/ABS1-22 and PC/ABS1-25, the cycles between two overload cycles are not large enough, the crack does not propagate out of the previous overload-affected zone before the successive overload is applied again, therefore the overload retardation ratio N_r/N_n can only be given approximately with the last

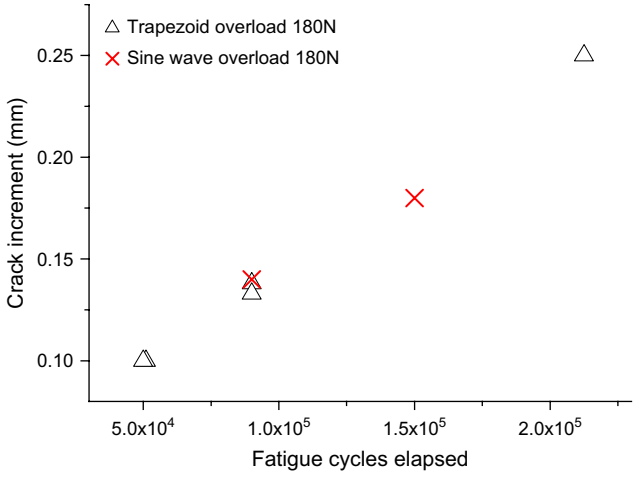

Fig. 9. The crack increment induced by overload vs the fatigue cycles elapsed between two overloads.

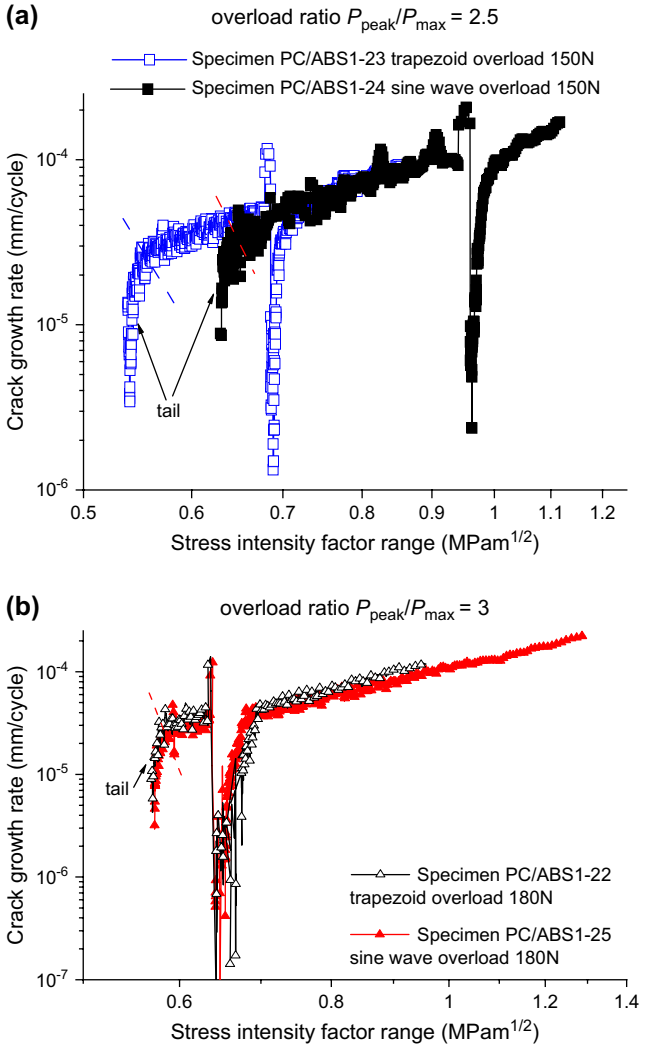

Fig. 10. Effect of overload on the da/dN–ΔK curve of PC/ABS alloy. (a) Overload ratio P_{peak}/P_{max} = 2.5 and (b) overload ratio P_{peak}/P_{max} = 3.

overload-affected retardation. With the same procedures as those for specimens PC/ABS1-23 and PC/ABS1-24, the overload retardation ratios N_r/N_n can be obtained to be 16.57 and 11.40 for specimens PC/ABS1-22 and PC/ABS1-25 which correspond to overload waveform of trapezoid and sinusoid, respectively. However, it should be noted that the results are given with only one specimen for each mechanical conditions, the repeatability of the results needs to be considered. As shown in Figs. 10 and 11, the normal fatigue crack propagation rates have not obvious difference for each specimens tested. Therefore, the repeatability of the test conditions is fairly good. The effect of overload ratio has larger effects on overload retardation ratios with the same tendency for the two overload waveform conditions. However, the overload waveform has only a little effect.

Up till now, it can be concluded that the overload waveform has slight effect, while the overload ratio has great effect on the crack growth retardation. Trapezoidal overload waveform results in slight longer delay of crack propagation in PC/ABS alloy than the sinusoidal overload waveform. In other words, trapezoidal overload waveform has a little stronger retardation effect than sinusoidal overload waveform for PC/ABS alloy. This might be due to the longer holding time of overload in the trapezoidal overload waveform, which leads to a little larger plastic zone at crack tip. It is also seen from Figs. 4 and 6–8 that the overload ratio has great effect on the fatigue crack growth retardation. The higher the overload ratio, the longer the retardation of crack propagation is, therefore the higher the overload retardation ratio.

According to Fig. 10, there is a "tail" stage in term of FCP rate for each specimen tested. Similar phenomena have also been observed in literature [5,7,12]. Although the loading conditions are different for each experiment, the phenomena are considered as crack growth inception [12] or near threshold stage [7] in literature. Because the initial crack is introduced by slowly pushing a fresh razor into the specimens in this experiment, it is natural to consider the plastic zone introduced during the crack initiation process as one of the reasons. But it is only a minor factor, because similar "tail" stages also appear when the specimens are previously fatigue cracked. The stepwise character of fatigue crack growth is considered as the sequential formation and fracture of craze damaged zones at crack tip [15]. Similarly, there would be a plastic deformation and/or damage accumulation process at crack tip in the crack initiation stage. Only little damage has been accumulated at a fresh crack tip before fatigue. As we learned from literature [30], cyclic loading can induce large number of tinny cracks near a defect or at crack tip, which leads to the reduction of fracture strain and to the brittleness of polymers. When the damage at crack tip is small, crack does not propagate or only propagate at very small growth rate during fatigue loading. FCP rate increases with the accumulation of the damage and plastic deformation, and reaches a normal crack growth level when a dynamic balance between the damage accumulation and crack growth has reached. After that, the normal FCP would continue until the dynamic process is disturbed.

Because the crack growth rate in the "tail" region and in the overload-affected zones could not reflect the normal fatigue crack growth rate level. After removing the crack growth data at these regions, Fig. 11 shows all the crack growth data of the five different PC/ABS specimens. Although the crack

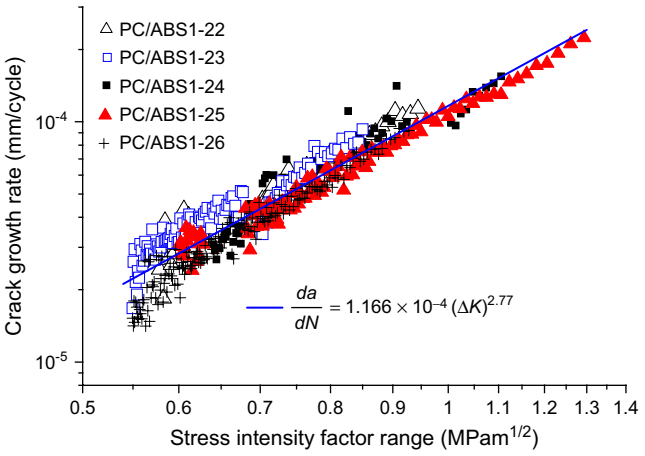

Fig. 11. The da/dN–ΔK curve of PC/ABS alloy.

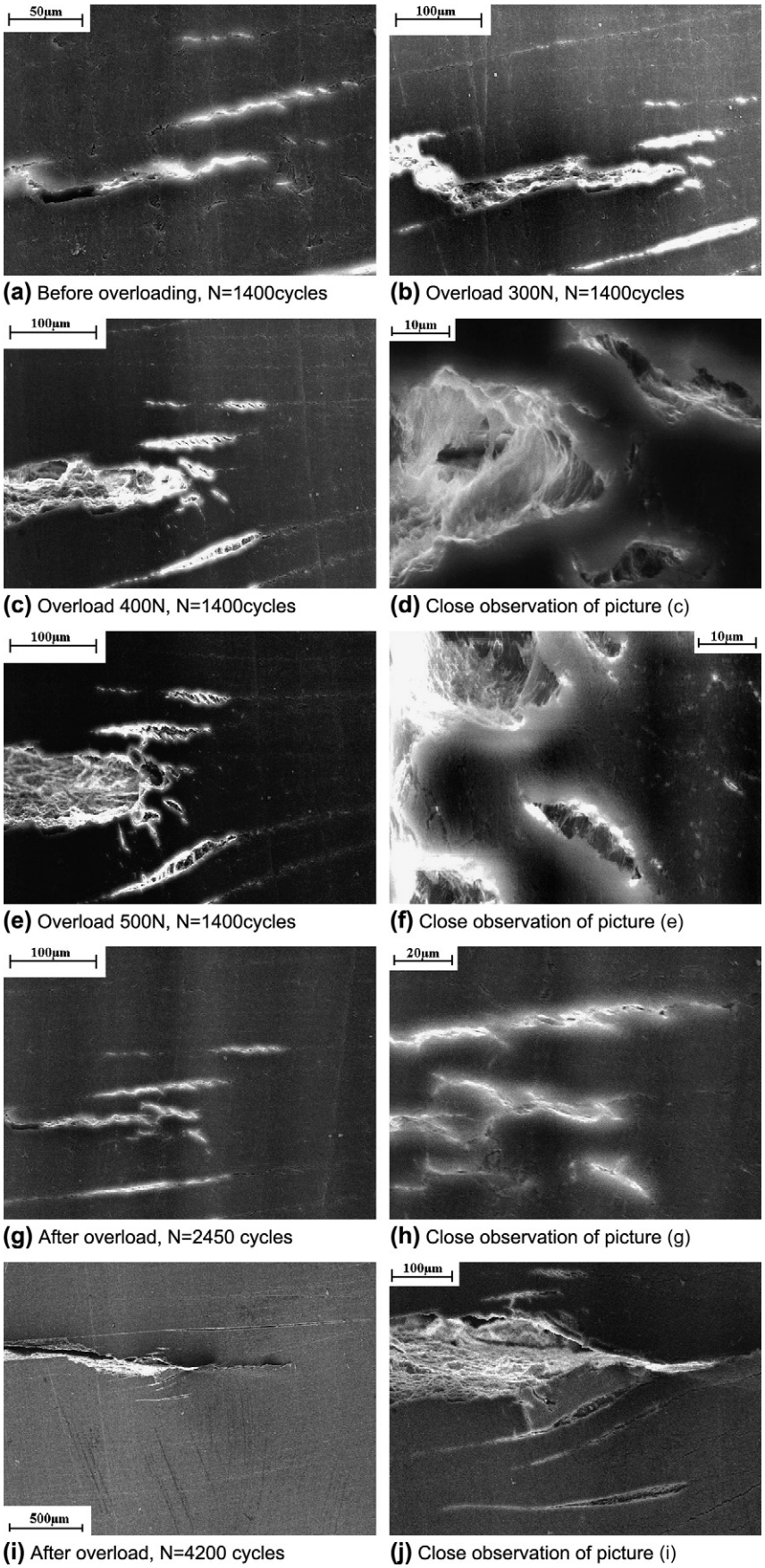

Fig. 12. In situ SEM observation of the crack tip during or after overload for eccentric tension specimen. (a) Before overloading, $N = 1400$ cycles; (b) overload 300 N, $N = 1400$ cycles; (c) overload 400 N, $N = 1400$ cycles; (d) close observation of picture (c); (e) overload 500 N, $N = 1400$ cycles; (f) close observation of picture (e); (g) after overload, $N = 2450$ cycles; (h) close observation of picture (g); (i) after overload, $N = 4200$ cycles; and (j) close observation of picture (i).

growth rates are more diversified in the small stress intensity factor region, it is clearly demonstrated that the steady state region conforms to the Pairs formula for the whole stress intensity factor range tested in the research with a small diversity. The fatigue crack propagation law for polymer PC/ABS at the test frequency of 3 Hz could be given with the test data from all the specimens for polymer PC/ABS as:

$$\frac{da}{dN} = 1.166 \times 10^{-4}(\Delta K)^{2.77} \quad (4)$$

Fig. 11 also shows the curve given by Eq. (4).

3.3. The micro-mechanism

It is well-known that the crack tip deformation pattern has great effect on the crack growth of polymers [15]. Therefore, it is useful to observe the crack tip deformation during FCP test for clear understanding of the FCP of PC/ABS alloy.

The in situ SEM micrographs in Fig. 12 show the micro-crack growth mechanisms before and after overloading for PC/ABS alloy obtained with the small SEM specimen shown in Fig. 1(b). The maximum and minimum fatigue loads P_{min} and P_{max} are 200 N and 20 N, and the fatigue load ratio and frequency are 0.1 and 0.08 Hz, respectively. Before the application of the overload, 1400 fatigue load cycles are applied to the small eccentric SEM specimen. Fig. 12(a) shows the microstructures at the fatigue crack tip. It is shown that some micro-cracks or crazes are observed here. Then an overload is applied to the specimen. The micro-cracks or crazes at the crack tip become larger as the load continues to increase. Fig. 12(b) shows the microstructures when the load increases to 300 N. Fig. 12(c) and (e) shows the microstructures when the load increases to 400 N and 500 N, respectively. Fig. 12(d) and (f) shows the corresponding close observation of Fig. 12(c) and (e). It is shown that the crazes or micro-cracks increase with the increasing load, and the fibrils in the crazes tend to be along with the tension direction, therefore perpendicular to the direction of crack propagation. We also learned from literature [31,32] that tension plastic deformation or cyclic true strains would make the polymer chains tend to be along with the tension direction. This would increase the resistance to FCP perpendicular to tension direction. After that, the load is reduced and the fatigue load of 20 N–200 N is applied again. Fig. 12(g) and (h) shows the microstructures at the crack tip after removing the overload. It is shown that a lot of crazes appear near the crack tip. The fatigue crack does not propagate in the next 2000 cycles. About 2500 cycles after overloading, the crack begins to propagate. Fig. 12(i) and (j) shows the microstructures of the crack tip at $N = 4200$ cycles. It is shown that the crack in the plastic zone is very thin, while the crack wake line before overloading is thick. It can also be learned from Fig. 12(i) and (j) that the subsequent deformation is much smaller in the overload-affected plastic zone. This is also supported by the measurement of crack tip stress given in Ref. [27]. It was found that the maximum stress would reduce just after removing the overload. That means much of the load is supported by the materials around the plastic zone; the stresses near the crack tip reduce significantly. This would reduce the FCP rate greatly. It can also be noted that the crack propagation line is thinner in the overload-affected plastic zone, which corresponds to smaller fatigue crack growth rates. This is consistent with the optical observation in Figs. 4–8.

Fig. 13 shows crazes generated in a normal FCP crack wake with a FCP rate of about 1.8×10^{-5} mm/cycle. It is shown that crazes restricted in a very narrow region near the crack. This means that there is only a limited plastic deformation at a normal FCP crack tip.

Fig. 14 shows the SEM observations of the crack propagation processes before and during overloading for specimen PC/ABS1-25, which correspond to the optical observation in Fig. 7. Fig. 14(a) shows the overview of the plastic zone A in Fig. 7, where A–C are plastic zones generated by overloads. It is shown that the crack propagation direction has changed due to each overloading. Fig. 14(b) shows the crazes generated near the crack just before and after overload. It is shown that there are only narrow zones where crazes are generated during normal fatigue crack growth process. However, there are a lot of crazes generated around the crack tip during overloading, therefore much larger plastic deformation is produced, which greatly relieves the stresses near the crack tip. Fig. 14(c) shows a close observation in the overload plastic zone near the crack at point P in Fig. 14(a). It is shown that larger crazes are generated ahead of the crack tip that would most likely be fractured during the subsequent fatigue loading. A lot of minor crazes are generated in the overload plastic zone. It is also shown that the crazes are mainly generated in the ABS particle rich regions. This means the ABS particles accelerate the crazing process in the PC/ABS alloy.

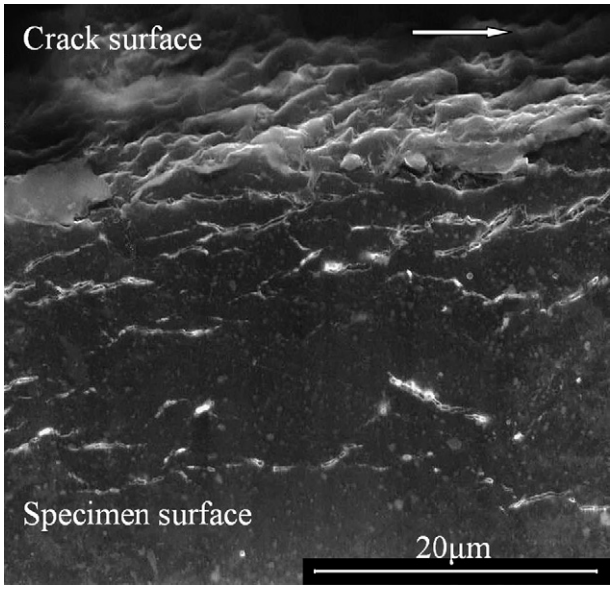

Fig. 13. Narrow craze zone formed near normal FCP crack with a FCP rate of about 1.8×10^{-5} mm/cycle. The arrow indicates the fatigue crack growth direction.

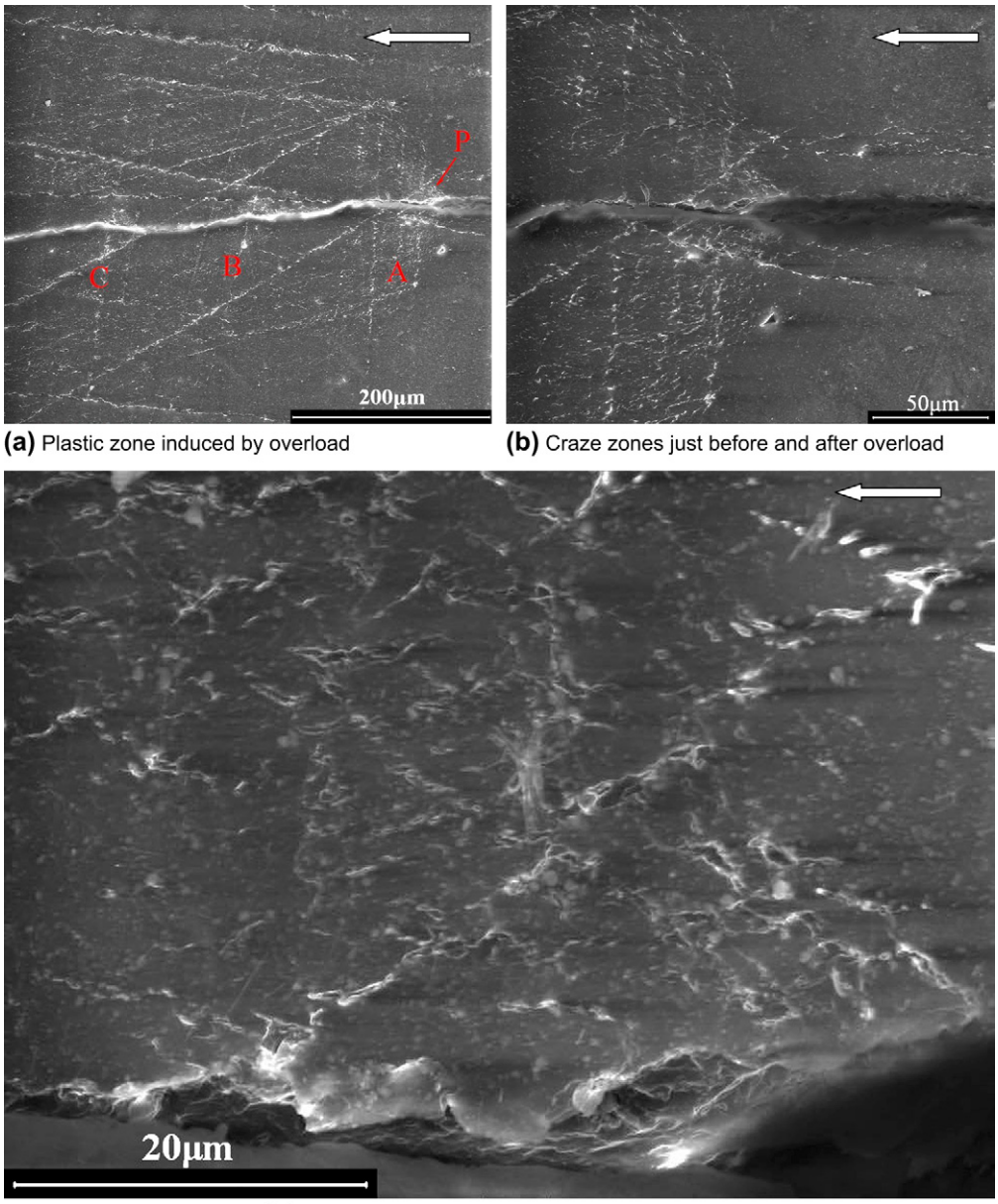

(a) Plastic zone induced by overload

(b) Craze zones just before and after overload

(c) Close observation of the overload plastic zone

Fig. 14. Crazes generated in the overload-affected plastic zone. The arrows indicate the fatigue crack growth direction. (a) Plastic zone induced by overload; (b) craze zones just before and after overload; and (c) close observation of the overload plastic zone.

It can be concluded from above observations that micro-cracks or crazes are observed within the porous structures near crack tip during fatigue loading. Much more crazes and/or micro-cracks appear near crack tip during and/or after overloading. The microstructures ahead of the crack tip are less stiff than the solid structures; therefore the stress amplitude near the crack tip is reduced after overloading. This might be one of the main reasons of the fatigue crack retardation.

Fig. 15 shows the fatigue crack surface character in the overload region for PC/ABS alloy. Fig. 15(a) shows the whole view of the six overload-affected zones for specimen PC/ABS1-22, which corresponds to the $a-N$ curve shown in Fig. 8. It is shown that stretched zones are generated for each overload application. Fig. 15(b) shows the stretched zone near point b in Fig. 15(a) due to the first overload. Large and rough tension dimple features are observed on the fracture surface in the stretched zone. This means that relatively larger plastic zone and more porous structures are generated in the stretched zone during the application of overload than that generated during constant fatigue loading for PC/ABS alloy. Fig. 15(c) shows the stretched zone near point c in Fig. 15(a) due to the fourth overload. It is seen that the dimples on the fracture surface in Fig. 15(c) are little smaller than that in Fig. 15(b). This is because the stretched zone in Fig. 15(c) is generated in a previous plastic and fatigue damaged zone, and the deformation is restricted by the previous plastic deformation. It can also be noted that there are a lot of particles in the dimples in Fig. 15(c). These should be ABS particles.

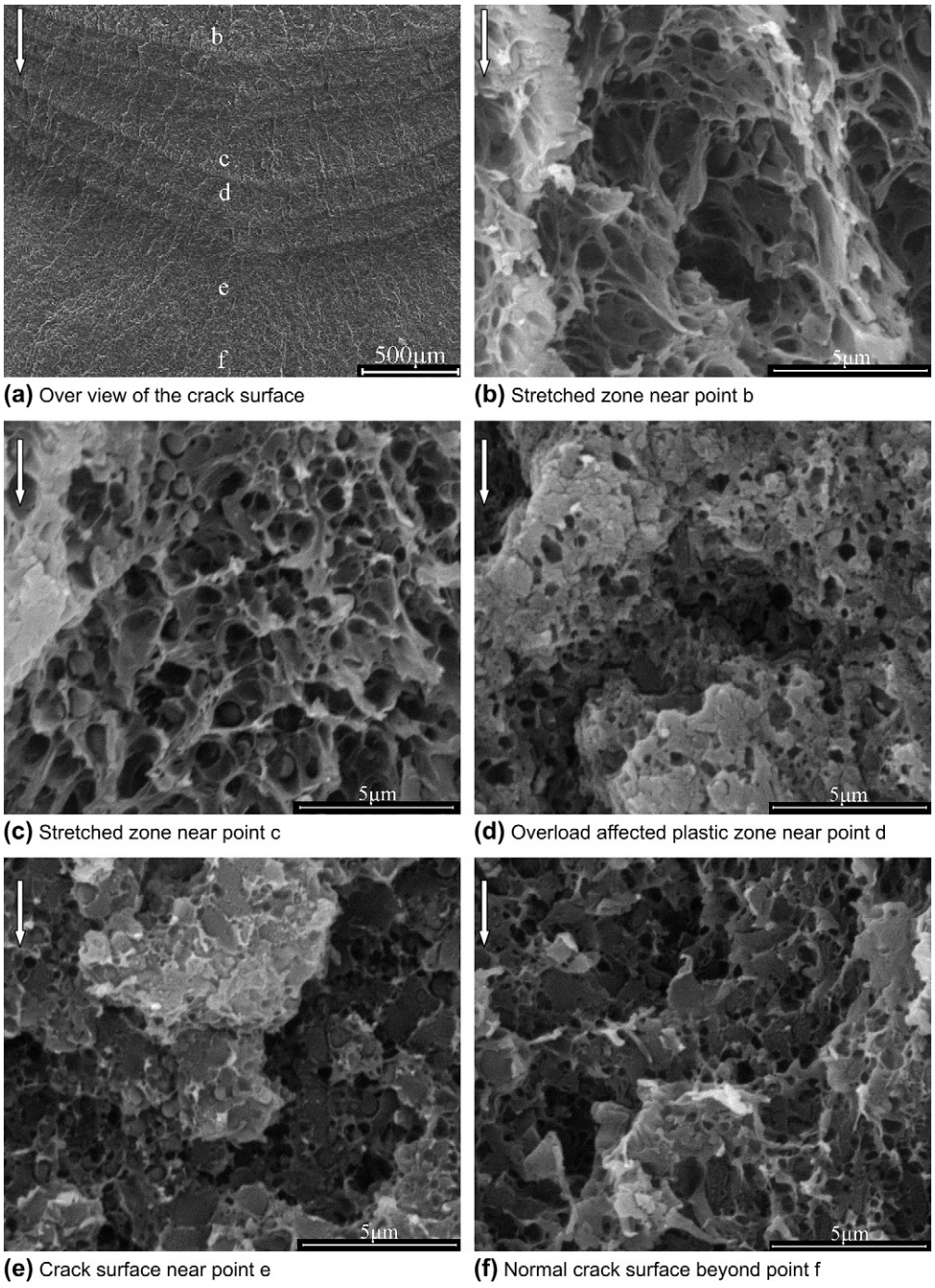

Fig. 15. SEM micrograph of the fatigue crack surface in the overload region for specimen PC/ABS1-22. The arrows indicate the fatigue crack growth direction. (a) Overview of the crack surface; (b) stretched zone near point b; (c) stretched zone near point c; (d) overload-affected plastic zone near point d; (e) crack surface near point e; and (f) normal crack surface beyond point f.

Debonding occurs between the body phase PC and ABS particles during the large deformation process. This relaxes local restriction and makes the PC phase deform easily. Therefore, a lot of crazes or micro-cracks are generated in the plastic zone. Particles can also be found in the dimples on the fracture surface in Fig. 15(b), but less frequently than that in Fig. 15(c). This means that some of the ABS particles might get off the dimples due to the larger deformation. The crazes in the overload-affected plastic zone would break when the fatigue duration is large enough, where the damage accumulation near the crack tip reaches a higher level. However, because the durations between the overloads are not long enough in this case, the crack growth does not reach the normal level before the subsequent overload is applied. Therefore, the crack growth rates are lower and the crack surfaces between the overload stretched zones are smoother. Fig. 15(d) shows the crack surface in the overload-affected zone near point d in Fig. 15(a). Smoother dimple fracture surface features are

shown in the overload-affected zone. This coincides with the thinner crack propagation line observed above. It should also be noted that there are a lot of ABS particles on the fracture surface, and parts of the surface are compressed during fatigue crack propagation. That means the fatigue crack is mainly fractured along the particle induced crazes in the overload-affected plastic zone, and there are some crack closure features between two crack or craze surfaces. This would reduce the stresses acted near the crack tip. During the fatigue damage accumulation stage, only small part of the fatigue load is applied to the damaged zone, and the fibrils in the craze damaged zone would gradually break as the fatigue test continues. Therefore, much lower FCP rate occurs in the period. The craze zone breaks when the next overload is applied to the specimen. Then a new stretched zone and plastic zone are produced. Fig. 15(e) shows the fatigue crack surface of about 0.6 mm from the last overload stretched zone near point e in Fig. 15(a), where the FCP rate is approaching the normal FCP rate (as shown in Fig. 8). It is seen that there are also some particles but no obvious crack surface closure is observed on the fracture surface. This means that the crack propagates in the crazes generated in the overload-affected plastic zone. Fig. 15(f) shows the normal fatigue crack surface beyond point f in Fig. 15(a). It is shown that the fracture surface is also dominated with dimple features, but no obvious ABS particles are found in the photos. This is because crack tip deformation is restricted to a very narrow region (Figs. 13 and 14(b)) near the crack in normal fatigue crack propagation process, therefore no enough particle debonding occurs in the plastic zone, so that higher crack growth rate is generated in the normal fatigue crack growth region than that in the overload-affected plastic zone, because most of the energy is used to make the crack propagate in normal FCP process.

Up till now, the overload effect on the fatigue process of PC/ABS alloy can be figured out. During normal fatigue crack process, the crack tip plastic zone is restricted in narrow regions, no enough plastic deformation or ABS particle debonding occurs, therefore a relative higher crack growth rate is generated. When an overload is applied during the normal fatigue loading process, a stretched zone is generated and a net crack increment occurs. A lot of crazes or micro-cracks are induced in the ABS particle rich region in the overload-affected plastic zone. These greatly relieve the stresses in the region near the crack tip, and absorb the energy extensively. Besides, crack surface closure also occurs in this stage. So that overload retardation occurs and much lower crack growth rate appears in the overload-affected plastic zone. Then, the crack growth rate increases gradually as the crack propagates out of the overload-affected plastic zone.

4. Conclusions

Overload effect on the fatigue crack propagation of PC/ABS alloy is experimentally investigated. An improved compliance method is employed to measure the crack propagation of PC/ABS alloy.

Overload waveform has a little effect on the FCP behavior of PC/ABS alloy. However, overload ratio has significant effect on the FCP behavior of PC/ABS alloy. Net increment of crack length is produced during overloading. Then, the FCP rates of polymers reduce to very low level and gradually increase to the normal level after the fatigue loading recovers. The higher the overload ratio, the bigger the FCP retardation of PC/ABS alloy.

Overload results in the blunt of crack tip and then the multiple micro-cracks and/or crazes near the crack tip are produced. These may greatly absorb the energy at crack tip and then greatly reduce FCP rate in polymers. The fractography of fatigue crack surfaces of PC/ABS alloy shows porous and/or dimple features. The stretched porous structures correspond to the blunting of the crack tip due to the overload. Smoother feature of the crack surface next to the stretched zones corresponds to the FCP retardation zone in the plastic zone induced by the overload.

Acknowledgements

This work is supported by the National Natural Science Foundation of China (10472087 and 10672129). The PC/ABS alloy was provided by Nanjing Julong Engineering Plastics Corporation.

References

[1] Bretz PE, Hertzberg RW, Manson JA. Polymer 1981;22:1272–8.
[2] Michel J, Manson JA, Hertzberg RW. Polymer 1984;25:1657–66.
[3] Lowe A, Kwon OH, Mai YW. Polymer 1996;37:565–72.
[4] Bureau MN, Dickson JI, Denault J. Journal of Materials Science 1998; 33:1405–19.
[5] Bureau MN, Dickson JI, Denault J. Journal of Materials Science 1998; 33:1591–606.
[6] Niinomi M, Wang L, Enjitsu T, Fukunaga KI. Journal of Materials Science: Materials Medicine 2001;12:267–72.
[7] Szabó JS, Gryshchuk O, Karger-Kocsis J. Journal of Materials Science Letters 2003;22:1141–5.
[8] Harcup JP, Duckett RA, Ward IM. Polymer Engineering and Science 2000;40:627–34.
[9] Harcup JP, Duckett RA, Ward IM. Polymer Engineering and Science 2000;40:635–44.
[10] Furmanski J, Pruitt LA. Polymer 2007;48:3512–9.
[11] Pruitt L, Bailey L. Polymer 1998;39:1545–53.
[12] Baker DA, Hastings RS, Pruitt L. Polymer 2000;41:795–808.
[13] Shah A, Steopanov EV, Hiltner A, Baer E, Klein M. International Journal of Fracture 1997;84:159–73.
[14] Shah A, Steopanov EV, Klein M, Hiltner A, Baer E. Journal of Materials Science 1998;33:3313–9.
[15] Parsons M, Stepanov EV, Hiltner A, Baer E. Journal of Materials Science 2000;35:2659–74.
[16] Favier V, Giroud T, Strijko E, Hiver JM, G'Sell C, Hellinckx S, et al. Polymer 2002;43:1375–82.
[17] Elinck JP, Bauwens JC, Homes G. International Journal of Fracture Mechanics 1971;7:227–87.
[18] Pulos GC, Knauss WG. International Journal of Fracture 1998;93:145–207.
[19] Ramsteiner F, Armbrust T. Polymer Testing 2001;20:321–7.
[20] Marissen R, Lange RFM, Biβels S, Hinkel P, Nowack H. International Journal of Fatigue 2005;27:71–84.
[21] Kim SH, Tai WP. Fatigue Fracture Engineering Materials Structure 1992;15(6):519–30.

[22] Borrego LP, Ferreira JM, Cruz JMP, Costa JM. Engineering Fracture Mechanics 2003;70:1379–97.
[23] Verma BB, Pandey RK. Journal of Materials Science 1999;34: 4867–71.
[24] Bathias C. International Journal of Fatigue 2006;28:1094–9.
[25] Mai YM. International Journal of Fracture 1979;15:R103–6.
[26] Pitoniak FJ, Grandt AF, Montulli LT, Packman PF. Engineering Fracture Mechanics 1974;6:663–70.
[27] Imai Y, Takase T, Nakano K. Journal of Materials Science 1989;24: 3289–94.
[28] Yuen BKC, Taheri F. Polymer Testing 2004;23:491–500.
[29] Fang QZ. Key Engineering Materials 2004;261/263:1179–84.
[30] Marissen R, Schudy D, Kemp AVJM, Coolen SMH, Duijzings WG, Van der Pol A, et al. Journal of Materials Science 2001;36:4167–80.
[31] Fang QZ, Wang TJ, Li HM. Polymer 2006;47:5174–81.
[32] Meyer RW, Pruitt LA. Polymer 2001;42:5293–306.